From microstructural features to effective toughness in disordered brittle solids

2014 EPL 105 34003

(http://iopscience.iop.org/0295-5075/105/3/34003)

A Letters Journal Exploring the Frontiers of Physics

February 2014

EPL, **105** (2014) 34003
doi: 10.1209/0295-5075/105/34003

www.epljournal.org

From microstructural features to effective toughness in disordered brittle solids

V. Démery[1(a)], A. Rosso[2] and L. Ponson[1]

[1] *Institut Jean Le Rond d'Alembert (UMR 7190), CNRS and Université Pierre et Marie Curie 75005 Paris, France*
[2] *Laboratoire Physique Théorique et Modèles Statistiques (UMR 8626), Université de Paris-Sud Orsay Cedex, France*

received 20 September 2013; accepted in final form 25 January 2014
published online 21 February 2014

PACS 46.50.+a – Fracture mechanics, fatigue and cracks
PACS 64.60.av – Cracks, sandpiles, avalanches, and earthquakes
PACS 68.35.Ct – Interface structure and roughness

Abstract – The relevant parameters at the microstructure scale that govern the macroscopic toughness of disordered brittle materials are investigated theoretically. We focus on a crack propagation that is planar and describe it as the motion of an elastic line within a plane with random distribution of toughness. Our study reveals two regimes: in the collective-pinning regime, the macroscopic toughness can be expressed as a function of a few parameters only, namely the average and the standard deviation of the local toughness distribution and the correlation lengths of the heterogeneous toughness field; in the individual-pinning regime, the passage from micro- to macro-scale is more subtle and the full distribution of local toughness is required to be predictive.

Bridging microscale features of materials with their macroscopic behavior is a major challenge for properties governed by the motion of interfaces. In brittle solids [1], ferromagnets [2], superconductors [3], thin film adhesives [4], or wetting films [5], impurities or defects present at the microstructure scale can produce dramatic macroscopic effects. They may also have interesting benefits: for example, large precipitate particles trap dislocations in metallic alloys, increasing their overall strength [6].

In this study, we address the deduction of the effective toughness of brittle solids from the variations of toughness at their microstructure scale. Failure processes involve in general complex mechanisms, such as damage and plastic deformations due to the high level of tensile stress in the crack tip vicinity, that are localized in the so-called process zone. A major simplification occurs in brittle solids where this zone is much smaller than the typical size of heterogeneities in the material. Assuming that the crack propagation is planar, it can be modeled as the overdamped motion of a line $u(r,t)$ in a two-dimensional heterogeneous medium [7–9], as represented in fig. 1. Previous works have investigated the effect of tough inclusions on the propagation of brittle cracks and were able to quantify the toughening induced by a periodic distribution of these obstacles [7,10]. Here, we focus on disordered microstructures, like randomly distributed impurities.

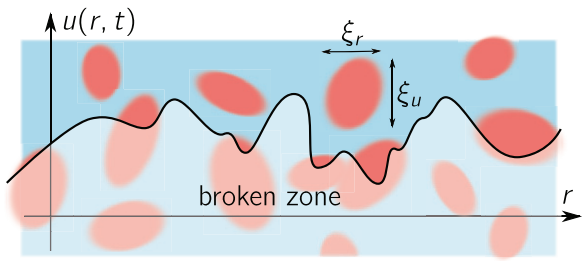

Fig. 1: (Color online) Crack front moving upwards in a disordered medium: red stands for tougher areas. The defects have characteristic sizes ξ_r and ξ_u in the r and u directions.

Earlier studies devoted to the propagation of an elastic line driven in a random medium have revealed a size-dependent crossover between a *weak-pinning* regime relevant for small systems and a *strong-pinning* regime that describes the thermodynamic limit [11–14]. For weak pinning, the macroscopic toughness is essentially the spatial average of the local toughness with a small, size-dependent, correction. For strong pinning, the failure

(a) E-mail: vincent.demery@polytechnique.edu

process is highly intermittent [15,16], and the avalanche-like dynamics results into a selection of some particularly strong regions within the fracture plane. The macroscopic toughness is thus larger than its spatial average.

We focus on the second case, and consider infinitely large specimens. Our study reveals two regimes, depending on the disorder amplitude: strongly disordered materials are in the *individual-pinning* regime, and their behavior depends on many microscopic parameters; the macroscopic toughness is shown to be dominated by the toughest obstacles. A regime of *collective pinning* occurs for a lower level of disorder, where the effective toughness is shown to depend on a few measurable microscopic parameters: the average and standard deviation of the local toughness distribution and the correlation lengths of the heterogeneous toughness field.

Our theoretical description of the crack evolution relies on two competing mechanisms: the material elasticity that tends to keep the front flat and the impurities that deform it. They reflect on the evolution equation of the front:

$$\frac{\partial u}{\partial t}(r,t) = K_{\rm ext} + \frac{c}{\pi}\int \frac{u(r',t)-u(r,t)}{(r'-r)^2}\mathrm{d}r' - K_{\rm c}(r,u). \quad (1)$$

The time has been rescaled by the front effective mobility. The macroscopic stress intensity factor $K_{\rm ext}$ is prescribed by the loading conditions of the sample; it will also be referred to as the *driving force*. The second term describes the distribution of stress intensity factor along the front resulting from its perturbed geometry [17]. This integral term represents long-range elastic interactions along the fracture line and also describes the behavior of wetting fronts [18]. The elastic constant is equal to $c = \langle K_{\rm c}\rangle/2$ for fracture fronts, but we keep it as a free parameter to make our study applicable to a broader class of systems. Finally, $K_{\rm c}(r,u)$ is the fluctuating local toughness.

The interplay between disorder and line elasticity determines the response of the line to an external force $K_{\rm ext}$: as long as the external force stays below a threshold $K_{\rm eff}$, the line remains *pinned* by the heterogeneities; when it exceeds $K_{\rm eff}$, the line *unpins* and acquires a non-zero asymptotic velocity [19]. To describe this behavior, it has been fruitful to consider the depinning transition as a critical phenomenon, with the velocity playing the role of an order parameter [19]. This analogy suggests that close to $K_{\rm eff}$ the front displays an universal behavior with critical exponents and scaling laws that have been extensively investigated [5,19–22]. If the test of these predictions in experiments has been rather successful [15,23,24], the most relevant quantity from an applied science perspective is the depinning threshold value $K_{\rm eff}$ which identifies with the macroscopic toughness. Analogously to the critical temperature in equilibrium phase transitions, $K_{\rm eff}$ is not universal and depends on the microscopic details of the system. The key point is what features at the microscopic scale affect the value of the critical driving force. To gain insight into this transition, we also study the front shape via its height-height correlation function, or *roughness*,

$$B(\delta r) = \overline{\langle [u(r)-u(r+\delta r)]^2\rangle}, \quad (2)$$

where $\langle\cdot\rangle$ and $\overline{\cdot}$ denote averages over the position r and the disorder realization, respectively.

We describe the material microstructure by rectangular domains of constant toughness. Their length is ξ_r in the r-direction; in the u-direction, it is drawn in an exponential distribution of average ξ_u. These rules set a particular disorder geometry; the effect of different spatial correlations along u will be discussed elsewhere. On each rectangular domain, the local toughness is $K_{\rm c} = \langle K_{\rm c}\rangle + \sigma k_{\rm c}$, where $k_{\rm c}$ is drawn from a symmetric probability distribution $P(k_{\rm c})$ of unit variance and zero mean value. The disorder is thus described by the standard deviation σ of the toughness distribution, the correlation lengths ξ_r and ξ_u and the probability distribution $P(k_{\rm c})$. The average toughness $\langle K_{\rm c}\rangle$ can be absorbed in the driving force and does not play any role in the study of eq. (1). In real materials, these parameters may be estimated. For instance, in a two-phase material with toughnesses $K_{\rm c}^1$ and $K_{\rm c}^2$ and densities n_1 and $n_2 = 1-n_1$, the disorder amplitude is $\sigma = \sqrt{n_1 n_2}|K_{\rm c}^1 - K_{\rm c}^2|$. The lengths ξ_r and ξ_u are given by the typical size of phase domains, as shown in fig. 1.

To identify the relevant parameters, we introduce the rescaled variables $\tilde r = r/\xi_r$, $\tilde u = u/\xi_u$ and $k_{\rm ext} = (K_{\rm ext} - \langle K_{\rm c}\rangle)/\sigma$. With these variables, eq. (1) reads, for a stationary state where $\partial u/\partial t = 0$,

$$0 = k_{\rm ext} - k_{\rm c}(\tilde r, \tilde u(\tilde r)) + \frac{1}{\pi}\frac{c\xi_u}{\sigma\xi_r}\int \frac{\tilde u(\tilde r') - \tilde u(\tilde r)}{(\tilde r'-\tilde r)^2}\mathrm{d}\tilde r'. \quad (3)$$

Thus, besides the disorder distribution $P(k_{\rm c})$, the behavior of eq. (3) depends only on the dimensionless parameter

$$\Sigma = \frac{\sigma\xi_r}{c\xi_u}, \quad (4)$$

hereafter referred to as the *disorder parameter*. The observables can then be written as functions of the disorder parameter and the disorder distribution multiplied by a numerical prefactor:

$$B(r) = \left(\frac{\sigma\xi_r}{c}\right)^2 b\left(\frac{r}{\xi_r}; \Sigma, P(k_{\rm c})\right), \quad (5)$$

$$\tilde K_{\rm eff} = K_{\rm eff} - \langle K_{\rm c}\rangle = \sigma k_{\rm eff}(\Sigma, P(k_{\rm c})). \quad (6)$$

To perform numerical simulations of eq. (1), the system is discretized in the r-direction with a step ξ_r and put on a strip of finite width L, with periodic boundary conditions. The driving force is replaced by a parabolic drive centered at w and of curvature κ: $K_{\rm ext} = \kappa[w - u(r,t)]$. We start with a flat configuration $u(r) = 0$ and set $w = w_0 > 0$. The line advances to a stable state $u_{w_0}(r)$ that can be found using the algorithm proposed in [25]. The stable configuration does not depend on the dynamics as soon as it satisfies the Middleton no-passing rule [26]; our dynamics, detailed in [25], satisfies this rule and is designed to

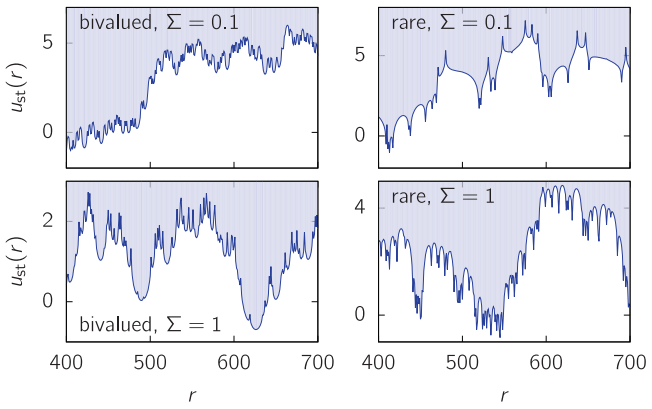

Fig. 2: (Color online) Stable front configurations for bivalued and rare disorder distributions and two values of the disorder parameter Σ, for $L = 1000$. The fronts propagate upwards.

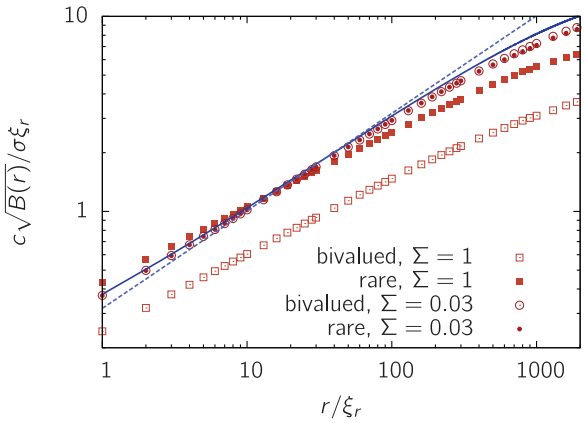

Fig. 3: (Color online) Crack front roughness: comparison between a bivalued (open symbols) and a rare distribution (full symbols), at low (circles) and high (squares) disorder. The average is performed over 100 fronts with $L = 10^4$ and $\kappa = 10^{-3}$. The solid line is the prediction (13) using Larkin's approximation and the dashed line the long-distance approximation (15).

converge rapidly to the first stable configuration. According to the no-passing rule [26], this stable configuration is independent of the initial configuration as soon as i) these configurations do not cross, if they do w_0 is increased; ii) there is no stable configuration $u^*(r)$ with $u^*(r) < 0$ for some r, this is satisfied if $\kappa w_0 \gg \sigma$. The pinning force acting on a stable line is measured as

$$K_{w_0}(\kappa) = \kappa \left[w_0 - \langle u_{w_0}(r) \rangle \right]. \tag{7}$$

Moving the parabola, we have computed 1000 stable configurations separated by several correlation lengths ξ_u so that their respective pinning forces are uncorrelated variables of average $\overline{K(\kappa)}$ and variance $\overline{\delta K(\kappa)^2}$.

The statistical tilt symmetry assures that the linear part of the equation of motion (and thus the curvature κ) is not renormalized [27]. This means that the length associated with the curvature $L_\kappa = c/\kappa$ fixes the distance from the critical point (located at $K_{\rm eff}$) as $\kappa^{1-\zeta}$. When $\kappa \to 0$ while $L \gg L_\kappa$, the average pinning force tends to the thermodynamical value, $K_{\rm eff}$, with finite-size effects of the form $\overline{K(\kappa)} = K_{\rm eff} + c_1 \kappa^{1-\zeta} + \cdots$ [28]. In the limit $L \gg L_\kappa = c/\kappa$, the interface can be modeled as a collection of independent interfaces of size L_κ and the central limit theorem assures that the variance $\overline{\delta K(\kappa)^2}$ should scale as $\sim (L_\kappa/L)\kappa^{2(1-\zeta)}$. This allows to write the finite-size effects without the exponent ζ,

$$\overline{K(\kappa)} = K_{\rm eff} + c_1 \sqrt{\kappa L \overline{\delta K(\kappa)^2}} + \cdots . \tag{8}$$

The value $K_{\rm eff}$ is extrapolated using eq. (8) and samples of size $L = 1000$ with κ ranging from 10^{-1} to 10^{-3}. The roughness $B(r)$ is obtained by averaging over 100 stable configurations with $L = 10^4$ and $\kappa = 10^{-3}$. Note that other finite-size procedures allow to extrapolate $K_{\rm eff}$. For example, one can compute the value of the critical force in samples of size $L \times L^\zeta$ and then take the limit $L \to \infty$. It has been shown recently that all these methods converge to the same value of $K_{\rm eff}$ [29], that is an intrinsic feature of the material. Here we use four different disorder distributions $P(k_c)$: bivalued, "rare" (with density $n = 0.1$)[1], Gaussian, and exponential. ξ_u is varied from 0.001 to 30 and σ from 1 to 8, and we set $c = 1$ and $\xi_r = 1$.

Examples of stable front configurations are shown in fig. 2, for bivalued and rare disorder distributions. The front amplitude does not depend on the disorder distribution $P(k_c)$ at low disorder ($\Sigma = 0.1$); on the contrary, it is larger for the rare distribution at high disorder ($\Sigma = 1$). These observations reflect in the roughness function given in fig. 3.

The disorder-induced toughening (or net critical driving force) $\tilde{K}_{\rm eff} = K_{\rm eff} - \langle K_c \rangle$ is plotted *vs.* the disorder parameter Σ in fig. 4; two regimes can be distinguished. At low disorder ($\Sigma < 1$), we observe a beautiful collapse between different disorder distributions: this is the *collective-pinning* regime. The net critical driving force follows the phenomenological law

$$\tilde{K}_{\rm eff} \simeq \frac{\sigma^2 \xi_r}{c \xi_u} = \sigma \Sigma. \tag{9}$$

This is our main result, justified later with physical arguments. On the contrary, at high disorder ($\Sigma > 1$), the net critical driving force depends strongly on the disorder distribution: this is the *individual-pinning* regime. In the limit $\Sigma \to \infty$, that can be interpreted as the limit $c \to 0$, the front is softer and has access to more and more disorder realizations. It may thus "choose" the most pinning one. As a result, when the disorder is a bounded distribution, the net critical driving force gets close to the bound. It is indeed what is observed for the bivalued distribution, whose maximum is 1, and for the "rare" distribution, whose maximum is $1/\sqrt{n} \simeq 3.16$. If the disorder is not bounded, the critical driving force is likely to diverge, as observed in the simulations. The fatter the distribution

[1] The rare distribution with a density n is defined by $P_{{\rm rare},n}(k_c) = (1-n)\delta(k_c) + \frac{n}{2}[\delta(k_c + \frac{1}{\sqrt{n}}) + \delta(k_c - \frac{1}{\sqrt{n}})]$.

tail is, the faster the divergence is expected; indeed, the divergence is faster for the exponential distribution than for the Gaussian one.

We now show that physical arguments adapted from the Larkin and Ovchinnikov study of vortex pinning in superconductors [3,30] allow for an intuitive interpretation of our results. The main difficulty in dealing with eq. (1) is its non-linearity coming from the disorder term. The first Larkin assumption is that this difficulty can be circumvented at *short distances*, where the crack front does not see that the disorder correlation length ξ_u is finite. The Larkin model is thus defined as the limit $\xi_u = \infty$ (*i.e.* $\Sigma = 0$), that amounts to removing the u-dependence of the disorder: $K_c(r,u) \to K_c(r)$ [30].

To allow comparison with the numerical simulations, we write the Larkin model for a line of length L discretized with a step a, with periodic boundary conditions and put in a parabola of curvature κ centered at $w = 0$. A stationnary solution satisfies

$$0 = -\kappa u_j + \frac{c}{\pi a} \sum_{j' \neq j} \phi_{j-j'} (u_{j'} - u_j) - K_{cj}, \tag{10}$$

where the elastic kernel

$$\phi_j = \sum_n \frac{1}{(j - nL/a)^2} \tag{11}$$

takes into account the periodic boundary conditions. In Fourier space, where $\tilde{u}_k = \sum_{j=0}^{N-1} \exp\left(-2\pi i \frac{jk}{N}\right) u_j$ ($N = L/a$ is the number of points of the line), the stationary condition (10) reads

$$-\kappa \tilde{u}_k + \frac{c}{\pi a} \left(\tilde{\phi}_k - \tilde{\phi}_0\right) \tilde{u}_k = -\tilde{K}_{ck}. \tag{12}$$

Extracting $\tilde{u}_k$ and computing the average $\overline{\tilde{u}_k \tilde{u}_{k'}}$ gives the roughness as a function of the disorder correlation. We choose a disorder correlation $\overline{K_{cj} K_{cj'}} = \sigma^2 \delta_{j,j'}$; in this case the discretization length sets the correlation length to $a = \xi_r$. The roughness at a distance $\delta r = aj$ is then

$$B_{\text{Larkin}}(aj) = \left(\frac{\sigma a}{c}\right)^2 \frac{2\pi^2}{N} \sum_k \frac{1 - \cos\left(\frac{2\pi jk}{N}\right)}{\left(\tilde{\phi}_0 - \tilde{\phi}_k + \frac{\pi\kappa a}{c}\right)^2}; \tag{13}$$

in the limit $\kappa \to 0$, $N \to \infty$, it becomes

$$B_{\text{Larkin}}(\delta r) = \left(\frac{\sigma}{c}\right)^2 \frac{a}{\pi} \int_{-\pi/a}^{\pi/a} \frac{1 - \cos(k\delta r)}{k^2 \left(1 - \frac{a|k|}{2\pi}\right)^2} \mathrm{d}k. \tag{14}$$

For distances short enough for the Larkin model to be relevant, but large compared to the disorder correlation length, $\delta r \gg a = \xi_r$, the roughness takes the form

$$B_{\text{Larkin}}(\delta r \gg \xi_r) \sim \left(\frac{\sigma \xi_r}{c}\right)^2 \frac{\delta r}{\xi_r}, \tag{15}$$

giving the Larkin roughness exponent $\zeta_{\text{Larkin}} = 0.5$.

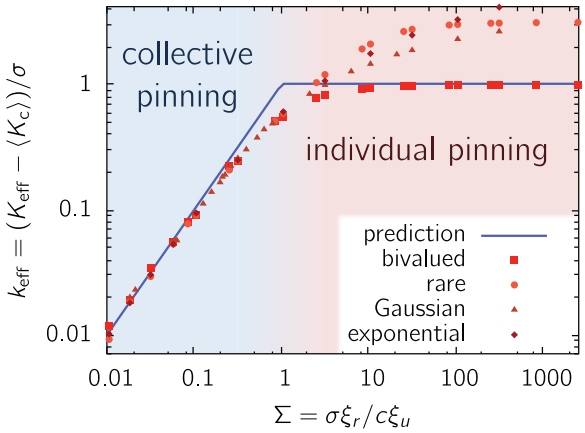

Fig. 4: (Color online) Dimensionless disorder-induced toughening $\tilde{k}_{\text{eff}}$ for different disorder distributions as a function of the disorder parameter Σ, extrapolated with (8) from 1000 samples of size $L = 1000$ with $10^{-3} \leq \kappa \leq 10^{-1}$. The line shows the prediction (20).

To explore the roughness below the correlation length, we need a disorder correlation function with correlation length larger than the discretization step, $\xi_r \gg a$. In practice, this cuts the integral in (14) at π/ξ_r, with an extra factor ξ_r/a. In the limit $\delta r \ll \xi_r$, it reduces to

$$B_{\text{Larkin}}(\delta r \ll \xi_r) \sim \left(\frac{\sigma}{c}\right)^2 \delta r^2 : \tag{16}$$

the line has a ballistic behavior at short distances.

The exact Larkin roughness (13) and its limiting law (15) are compared to the numerical simulations in fig. 3. At low disorder, the agreement between simulations and the Larkin prediction is strikingly good. The long-distance approximation is also rather good. At high disorder, as expected, the results are far from the prediction.

We can address the question of the validity of the Larkin regime: what does the assumption of "short distances" mean? If the amplitude of the front perturbations characterized by the roughness is smaller than the correlation length ξ_u, the Larkin model should represent correctly the behaviour of the line; on the contrary, when it is larger than ξ_u, a different behaviour is expected. This defines the length in the r-direction up to which the Larkin approximation is relevant, the so-called *Larkin length* L_c (see ref. [31] for a recent review), by

$$\sqrt{B_{\text{Larkin}}(L_c)} = \xi_u. \tag{17}$$

If the Larkin length is larger than the correlation length ξ_r, its expression can be derived from eq. (15):

$$L_c = \left(\frac{c\xi_u}{\sigma\xi_r}\right)^2 \xi_r = \frac{\xi_r}{\Sigma^2}. \tag{18}$$

The domains of size L_c that behave as if ξ_u was infinite are called *Larkin domains*; in these domains and for distances larger than ξ_r, the roughness is given by (15). For larger

distances, the roughness departs from the Larkin prediction and continuity implies

$$B(\delta r \gg L_{\rm c}) \simeq \xi_u (\delta r/L_{\rm c})^{\zeta}, \tag{19}$$

with a roughness exponent $\zeta \simeq 0.39$ [25].

The second Larkin assumption is that the critical driving force is given by the typical toughness seen by a Larkin domain. The toughness averaged along the line on a Larkin domain has a mean $\langle K_{\rm c}\rangle$ and its standard deviation depends on $L_{\rm c}$:

- if $L_{\rm c} > \xi_r$ (or $\Sigma < 1$), a Larkin domain sees several defects: this is the *collective-pinning* regime. The local toughness is averaged over $L_{\rm c}/\xi_r$ uncorrelated defects and the standard deviation is $\sigma\sqrt{\xi_r/L_{\rm c}}$, leading to the net critical driving force $\tilde{K}_{\rm eff} = \sigma\sqrt{\xi_r/L_{\rm c}}$.
- if $L_{\rm c} < \xi_r$ (or $\Sigma > 1$), a Larkin domain sees only one defect: this is the *individual-pinning* regime. The standard deviation is σ, giving the net critical driving force $\tilde{K}_{\rm eff} = \sigma$.

Using the long-distance expression of the Larkin length (18), we can write explicitly the net critical driving force

$$\tilde{K}_{\rm eff} = \begin{cases} \dfrac{\sigma^2\xi_r}{c\xi_u} = \sigma\Sigma, & \text{if } \Sigma = \dfrac{\sigma\xi_r}{c\xi_u} < 1, \\ \sigma, & \text{if } \Sigma = \dfrac{\sigma\xi_r}{c\xi_u} > 1. \end{cases} \tag{20}$$

These expressions are compared to the simulations for the four different disorder distributions in fig. 4. In the collective-pinning regime, the prevision captures the results of the simulations: this confirms the validity of eq. (9), irrespective of the underlying local toughness distribution. In the individual-pinning regime, the prediction (20) does not fully describe the results of the simulations, but provides a lower-bound for the effective toughness:

$$K_{\rm eff} \geq \langle K_{\rm c}\rangle + \sigma. \tag{21}$$

Indeed, in this regime, the toughest defects that set the value of the critical force are systematically tougher than the toughness standard deviation σ.

As a possible application, we consider the case of a material of toughness $K_{\rm c}^1$ reinforced by a small volume fraction $n_2 \ll 1$ of randomly distributed particles with large toughness $K_{\rm c}^2$ and define the contrast as $C = (K_{\rm c}^2 - K_{\rm c}^1)/K_{\rm c}^1$. For an isotropic distribution of particles ($\xi_r = \xi_u$), eq. (20) predicts an increase of the effective toughness of the material by a factor $K_{\rm eff}/K_{\rm c}^1 \simeq 1 + n_2(C + 2C^2)$ in the collective regime. This result is quite different from the predictions of refs. [7,10] obtained for a periodic array of tough particles where $K_{\rm eff}/K_{\rm c}^1 \simeq 1 + 2C\sqrt{n_2/\pi}$, highlighting the crucial role played by disorder.

We underline the limitations of the line model used here in the context of fracture. It rests on two assumptions: i) The solid is brittle, *i.e.* the process zone is small compared to the microstructural length scales ξ_r and ξ_u. This allows to treat the crack front as a line that separates the fracture plane into two distinct domains of intact and broken material. ii) The distortion of the line is small enough so that the linear interaction term used in eq. (1) describes properly the line elasticity. This condition is fullfilled as long as the steepest slopes along the crack line are smaller than one. The steepest slopes are found at small distances, for $\delta r \ll \xi_r, L_{\rm c}$, where the ballistic roughness (16) shows that they are $[\sqrt{B(\delta r)}/\delta r]_{\rm max} \simeq \sigma/c$. The condition $\sigma/c \leq 1$, or $\sigma \leq \langle K_{\rm c}\rangle/2$, limits our study to moderately heterogeneous solids, where the spatial toughness variations are smaller than the average toughness. This condition is generally satisfied in the collective-pinning regime, whereas in the individual-pinning regime where $\sigma/c > \xi_u/\xi_r$ (eq. (20)), it can be only satisfied for anisotropic disorder with $\xi_r > \xi_u$. Beyond the assumption ii), larger local slopes of order one would require non-linear corrections to the line elasticity [32]. However, we expect a similar toughening mechanism governed by the toughest defects to apply. If the steepest slopes are even larger, the line model (assumption i)) breaks down: this may come from crack bridging due to very tough inclusions [10,33] that conserve clusters of intact material in the broken domain; or from the nucleation and coalescence of damage ahead of the crack that occurs, *e.g.*, in quasi-brittle solids. In this latter case, the front becomes fractal [34] and a material description based on random networks of fuses or springs will be more appropriate [35].

We now compare the regimes identified here to those observed in former studies. In the self-coherent schemes [12,14], the weak- to strong-pinning transition corresponds to the emergence of metastability: for small systems or low disorder, there is no metastability and the effective toughness is equal to the space-averaged toughness; for large systems or strong disorder, metastability produces a disorder-induced toughening. The transition depends on the system size and the weak-pinning regime disappears in the thermodynamic limit. In our case, metastability is always present, indicating that the individual- and collective-pinning regimes belong to the strong-pinning regime. The individual- to collective-pinning crossover occurs when the Larkin length $L_{\rm c}$ equals the disorder correlation length ξ_r. We can expect that the pinning becomes weak when the Larkin length exceeds the system size L. The system size then sets the size of the Larkin domains, leading to a disorder-induced toughening,

$$\tilde{K}_{\rm eff} = \sigma\sqrt{\frac{\xi_r}{L}}. \tag{22}$$

This regime occurs for very low disorder $\sigma < c\xi_u/\sqrt{L\xi_r}$ and has a small effect on the material toughness; this explains why it has been neglected in some studies [12,14].

In the linear stability analysis [13], the different behaviors show up in the *participation ratio* τ of the most

unstable mode. In the weak-pinning regime, the system unpins as a whole and $\tau \simeq 1$; in the strong-pinning regime, the avalanches are concentrated on a small portion of the system and $\tau < 1$. Following Larkin's argument, the Larkin length is also the minimal size of avalanches and is thus linked to the participation ratio via $\tau = L_c/L$. With this interpretation, a participation ratio in the range $\xi_r/L < \tau < 1$ reveals a collective regime, while $\tau \simeq \xi_r/L$ is the signature of individual pinning. However, the connection between the participation ratio and the Larkin length deserves further investigations, as emphasized in [13].

Finally, our study provides also insights into the behavior of contact lines that follow the same evolution equation as crack lines. In refs. [36,37], the disorder amplitude can be computed from the defects density n and strength h as $\sigma^2 \sim nh^2$, while the capillary length sets the system size L. The hysteresis H in wetting problems is analogous to the disorder-induced toughening $\tilde{K}_{\text{eff}}$ for cracks. First, it was found that the hysteresis is zero for a defect strength h below a critical value h_c; that corresponds to the weak-pinning regime. As noted in [37], this regime disappears when the capillary length goes to infinity. In addition, the scaling $h_c(n) \sim 1/\sqrt{n}$ is consistent with the weak- to strong-pinning crossover occurring for $L = L_c = c^2\xi_r/(nh^2)$, as suggested here. Above this critical value, but at low densities, the hysteresis scales as $H \sim nh^2 \sim \sigma^2$: this behavior is consistent with the collective-pinning regime in eq. (20).

To conclude, we have investigated the effect of a disordered microstructure on the pinning of a brittle crack front. We have shown that the interaction between the front and the disorder is governed by one dimensionless parameter and that two distinct regimes can be identified. In the collective-pinning regime that occurs at low-disorder amplitude, many impurities act together to pin the crack front. The effective toughness follows eq. (9) and depends on a few parameters measurable from the material microstructure. On the other hand, at high-disorder amplitude, the front is pinned by tough individual defects: this is the individual-pinning regime. The macroscopic toughness is shown to depend on many parameters, such as the actual distribution of microscopic local toughness.

* * *

The authors would like to thank J.-B. Leblond, V. Lecomte, N. Pindra and S. Roux for fruitful discussions.

REFERENCES

[1] Bonamy D. and Bouchaud E., *Phys. Rep.*, **498** (2011) 1.

[2] Zapperi S., Cizeau P., Durin G. and Stanley H. E., *Phys. Rev. E*, **58** (1998) 6353.

[3] Larkin A. I. and Ovchinnikov Y. N., *J. Low Temp. Phys.*, **34** (1979) 409.

[4] Xia S., Ponson L., Ravichandran G. and Bhattacharya K., *Phys. Rev. Lett.*, **108** (2012) 196101.

[5] Moulinet S., Rosso A., Krauth W. and Rolley E., *Phys. Rev. E*, **69** (2004) 035103.

[6] Callister W. D., *Fundamentals of Materials Science and Engineering* (Wiley & Sons) 2012.

[7] Gao H. and Rice J. R., *J. Appl. Mech.*, **56** (1989) 828.

[8] Schmittbuhl J., Roux S., Vilotte J. P. and Måløy K. J., *Phys. Rev. Lett.*, **74** (1995) 1787.

[9] Ponson L. and Bonamy D., *Int. J. Fract.*, **162** (2010) 21.

[10] Bower A. F. and Ortiz M., *J. Mech. Phys. Solids*, **39** (1991) 815.

[11] Tanguy A., Gounelle M. and Roux S., *Phys. Rev. E*, **58** (1998) 1577.

[12] Roux S., Vandembroucq D. and Hild F., *Eur. J. Mech. A*, **22** (2003) 743.

[13] Tanguy A. and Vettorel T., *Eur. Phys. J. B*, **38** (2004) 71.

[14] Patinet S., Vandembroucq D. and Roux S., *Phys. Rev. Lett.*, **110** (2013) 165507.

[15] Bonamy D., Santucci S. and Ponson L., *Phys. Rev. Lett.*, **101** (2008) 045501.

[16] Måløy K. J., Santucci S., Schmittbuhl J. and Toussaint R., *Phys. Rev. Lett.*, **96** (2006) 045501.

[17] Rice J. R., *J. Appl. Mech.*, **52** (1985) 571.

[18] Joanny J. F. and de Gennes P. G., *J. Chem. Phys.*, **81** (1984) 552.

[19] Narayan O. and Fisher D. S., *Phys. Rev. B*, **48** (1993) 7030.

[20] Nattermann T., Stepanow S., Tang S. and Leschhorn H., *J. Phys. II*, **2** (1992) 1483.

[21] Le Doussal P., Wiese K. J. and Chauve P., *Phys. Rev. B*, **66** (2002) 174201.

[22] Bustingorry S., Kolton A. B. and Giamarchi T., *EPL*, **81** (2008) 26005.

[23] Ponson L., *Phys. Rev. Lett.*, **103** (2009) 055501.

[24] Santucci S. *et al.*, *Eur. Phys. J.*, **92** (2010) 44001.

[25] Rosso A. and Krauth W., *Phys. Rev. E*, **65** (2002) 025101(R).

[26] Middleton A. A., *Phys. Rev. Lett.*, **68** (1992) 670.

[27] Schulz U., Villain J., Brézin E. and Orland H., *J. Stat. Phys.*, **51** (1988) 1-27

[28] Rosso A., Doussal P. L. and Wiese K. J., *Phys. Rev. B*, **75** (2007) 220201.

[29] Kolton A. B., Bustingorry S., Ferrero E. E. and Rosso A., *J. Stat. Mech.* (2013) 12004.

[30] Larkin A. I., *Sov. Phys. JETP*, **31** (1970) 784.

[31] Agoritsas E., Lecomte V. and Giamarchi T., *Physica B: Condens. Matter*, **407** (2012) 1725.

[32] Vasoya M., Leblond J.B. and Ponson L., *Int. J. Solids Struct.*, **50** (2013) 371.

[33] Budiansky B., Amazigo J. and Evans A. G., *J. Mech. Phys. Solids*, **36** (1988) 167.

[34] Gjerden K. S., Stormo A. and Hansen A., *Phys. Rev. Lett.*, **111** (2013) 135502

[35] Moreira A. A., Oliveira C. L. N., Hansen A., Araújo N. A. M., Herrmann H. J. and Andrade J. S., *Phys. Rev. Lett.*, **109** (2012) 255701

[36] Di Meglio J.-M., *Europhys. Lett.*, **17** (1992) 607.

[37] Crassous J. and Charlaix E., *Europhys. Lett.*, **28** (1994) 415.